Asociación Argentina
de Mecánica Computacional

Mecánica Computacional Vol XXVI, pp.1055-1074
Sergio A. Elaskar, Elvio A. Pilotta, Germán A. Torres (Eds.)
Córdoba, Argentina, Octubre 2007

COMPARISON AMONG STRUCTURED HIGH RESOLUTION ALGORITHMS IN THE SOLUTION OF THE EULER EQUATIONS IN TWO-DIMENSIONS

Edisson Sávio de Góes Maciel[a]

[a]*CNPq Researcher, Rua Demócrito Cavalcanti, 152, Afogados, Recife, Pernambuco, Brazil, 50750-080, saviomaciel@pq.cnpq.br*

Keywords: Yee, Warming and Harten algorithm, Harten algorithm, Yee and Kutler algorithm, Hughson and Beran algorithm, Euler equations.

Abstract. The present work compares the Yee, Warming and Harten, the Harten, the Yee and Kutler and the Hughson and Beran high resolution schemes applied to the solution of aeronautical and aerospace problems. All schemes are TVD flux difference splitting type and are second order accurate in space. The Euler equations in conservative form, employing a finite volume formulation and a structured spatial discretization, are solved in two-dimensions. The time integration is performed by a time splitting method and is first order accurate. The steady state physical problems of the supersonic flows along a ramp and around a blunt body configuration are studied. In the ramp problem, the Hughson and Beran scheme was the most critical because presented the most severe pressure field and the most intense Mach number field in relation to the others schemes. The shock and the expansion fan are better captured by the Yee, Warming and Harten and the Yee and Kutler schemes. The Harten and the Hughson and Beran schemes presented better pressure distribution than the others schemes when compared with the theory. The shock angle was best estimated by the Harten scheme. In the blunt body problem, the Harten scheme presented the most severe pressure field in relation to the others schemes. The aerodynamic coefficient of lift was better estimated in the solutions generated by the Harten and the Hughson and Beran schemes. The stagnation pressure ahead of the configuration is best predicted by the Harten scheme. As conclusion, the Harten scheme presents the most accurate solutions in comparison with the others schemes in both examples studied in this work, as well the most severe pressure field in the blunt body problem, high supersonic flow, characterizing it as the most conservative in relation to the others schemes to this type of flow, which indicates this one as a good scheme to the prediction of flow properties in the project phase of aerospace vehicles.

1 INTRODUCTION

High resolution upwind schemes have been developed since 1959, aiming to improve the generated solution quality, yielding more accurate solutions and more robust codes. The high resolution upwind schemes can be of flux vector splitting type or flux difference splitting type. In the former case, more robust algorithms are yielded, while in the later case, more accuracy is obtained. Several studies were reported involving high resolution algorithms in the international literature, as for example:

Roe (1981) presented a work that emphasized that several numerical schemes to the solution of the hyperbolic conservation equations were based on exploring the information obtained in the solution of a sequence of Riemann problems. It was verified that in the existent schemes the major part of this information was degraded and that only certain solution aspects were solved. It was demonstrated that the information could be preserved by the construction of a matrix with a certain "U property". After the construction of this matrix, its eigenvalues could be considered as wave velocities of the Riemann problem and the U_L-U_R projections over the matrix's eigenvectors are the jumps which occur between intermediate stages.

Yee, Warming and Harten (1982) implemented a high resolution second order explicit method based on Harten's ideas. The method had the following properties: (a) the scheme was developed in conservation form to ensure that the limit was a weak solution; (b) the scheme satisfied a proper entropy inequality to ensure that the limit solution would have only physically relevant discontinuities; and (c) the scheme was designed such that the numerical dissipation produced highly accurate weak solutions. The method was applied to the solution of a quasi-one-dimensional nozzle problem and to the two-dimensional shock reflection problem, yielding good results. An implicit implementation was also investigated to one- and two-dimensional cases.

Harten (1983) developed a class of new finite difference schemes, explicit and with second order of spatial accuracy to calculation of weak solutions of the hyperbolic conservation laws. These schemes highly non-linear were obtained by the application of a first order non-oscillatory scheme to an appropriated modified flux function. The so derived second order schemes reached high resolution, while preserved the robustness property of the original non-oscillatory scheme.

Yee and Kutler (1985) presented a work which extended the Harten (1983) scheme to a generalized coordinate system, in two-dimensions. The method called "TVD scheme" by the authors was tested to the physical problem of a moving shock impinging a cylinder. The numerical results were compared with the MacCormack (1969) scheme, presenting good results.

Hughson and Beran (1991) proposed an explicit, second order accurate in space, TVD ("Total Variation Diminishing") scheme to solve the Euler equations in axis-symmetrical form, applied to the studies of the supersonic flow around a sphere and the hypersonic flow around a blunt body. The scheme was based on the modified flux function approximation of Harten (1983) and its extension from the two-dimensional space to the axis-symmetrical treatment was developed. Results were compared to the MacCormack (1969) algorithm's solutions. High resolution aspects, capability of shock capture and robustness properties of this TVD scheme were investigated.

In this work, the Yee, Warming and Harten (1982), the Harten (1983), the Yee and Kutler (1985) and the Hughson and Beran (1991) schemes are implemented, on a finite volume context and using an upwind and a structured spatial discretization, to solve the Euler equations, in two-dimensions, and are compared with themselves. All schemes are second

order accurate in space and are applied to the solution of the supersonic flows along a ramp and around a blunt body configuration. A spatially variable time step procedure is implemented aiming to accelerate the convergence of the schemes to the steady state condition. The effective gains in terms of convergence ratio with this procedure are reported in Maciel (2005). The results have demonstrated that the Hughson and Beran (1991) scheme yields the most severe results in the ramp problem, while the Harten (1983) scheme yields the most accurate results in both problems and the most severe results in the blunt body problem, indicating this scheme, a priori, as the best choice in relation to the tested schemes to simulate supersonic flows. More complete studies, involving more different physical problems, are aimed by this author with the intention of better highlighting the characteristics of these schemes.

The motivation and justification of this work is to present TVD high resolution schemes, which are reported in the CFD literature as able to provide numerical solutions free of oscillations, on a finite volume context and test their abilities to provide good shock capturing properties. Furthermore, the CFD literature describes these schemes on a finite difference context and using a generalized coordinate system. Hence, this work represents an original contribution in the sense that the studied TVD schemes are described and implemented on a finite volume context.

2 EULER EQUATIONS

The fluid movement is described by the Euler equations, which express the conservation of mass, of linear momentum and of energy to an inviscid, heat non-conductor and compressible mean, in the absence of external forces. In the integral and conservative forms, these equations can be represented by:

$$\partial/\partial t \int_V Q dV + \int_S \left(E_e n_x + F_e n_y\right) dS = 0\,, \tag{1}$$

where Q is written to a Cartesian system, V is a cell volume, n_x and n_y are the components of the normal unity vector to the flux face, S is the surface area and E_e and F_e represent the components of the convective flux vector. Q, E_e and F_e are represented by:

$$Q = \begin{Bmatrix} \rho \\ \rho u \\ \rho v \\ e \end{Bmatrix}, \quad E_e = \begin{Bmatrix} \rho u \\ \rho u^2 + p \\ \rho uv \\ (e+p)u \end{Bmatrix} \quad \text{and} \quad F_e = \begin{Bmatrix} \rho v \\ \rho uv \\ \rho v^2 + p \\ (e+p)v \end{Bmatrix}, \tag{2}$$

being ρ the fluid density; u and v the Cartesian components of the velocity vector in the x and y directions, respectively; e the total energy per unity volume of the fluid mean; and p the static pressure of the fluid mean.

In all problems, the Euler equations were nondimensionalized in relation to the freestream density, ρ_∞, and in relation to the freestream speed of sound, a_∞. The matrix system of the Euler equations is closed with the state equation of a perfect gas:

$$p = (\gamma - 1)\left[e - 0.5\rho(u^2 + v^2)\right] \tag{3}$$

and γ being the ratio of specific heats. The total enthalpy is determined by $H = (e+p)/\rho$.

3 YEE, WARMING AND HARTEN (1982) ALGORITHM

The Yee, Warming and Harten (1982) algorithm, second order accurate in space, is specified by the determination of the numerical flux vector at *(i+½,j)* interface.

Following a finite volume formalism, which is equivalent to a generalized system, the right and left cell volumes, as well the interface volume, necessaries to coordinate change, are defined by:

$$V_R = V_{i+1,j}\,,\quad V_L = V_{i,j} \quad \text{and} \quad V_{int} = 0.5\left(V_R + V_L\right), \tag{4}$$

in which "*R*" and "*L*" represent right and left states, respectively. The cell volume is defined by:

$$\begin{aligned} V_{i,j} = 0.5\Big|&\left(x_{i,j} - x_{i+1,j}\right)y_{i+1,j+1} + \left(x_{i+1,j} - x_{i+1,j+1}\right)y_{i,j} + \left(x_{i+1,j+1} - x_{i,j}\right)y_{i+1,j}\Big| + \\ 0.5\Big|&\left(x_{i,j} - x_{i+1,j+1}\right)y_{i,j+1} + \left(x_{i+1,j+1} - x_{i,j+1}\right)y_{i,j} + \left(x_{i,j+1} - x_{i,j}\right)y_{i+1,j+1}\Big|, \end{aligned} \tag{5}$$

where a computational cell and its flux surfaces are defined in Fig. 1.

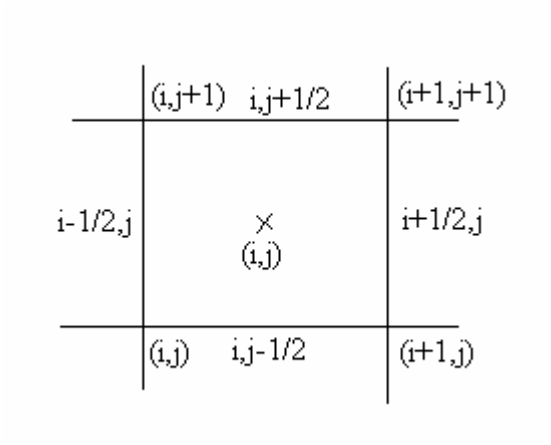

Figure 1: Computational cell.

The area components at interface are defined by: $S_{x\_\text{int}} = s_x^{'} S$ and $S_{y\_\text{int}} = s_y^{'} S$, where $s_x^{'}$ and $s_y^{'}$ are defined as: $s_x^{'} = s_x / S$ and $s_y^{'} = s_y / S$, being $S = \left(s_x^2 + s_y^2\right)^{0.5}$. Expressions to s_x and s_y, which represent the S_x and S_y components always adopted in the positive orientation, are given in Tab. 1.

Surface	s_x	s_y
i,j-1/2	$-\left(y_{i+1,j} - y_{i,j}\right)$	$\left(x_{i+1,j} - x_{i,j}\right)$
i+1/2,j	$\left(y_{i+1,j+1} - y_{i+1,j}\right)$	$\left(x_{i+1,j} - x_{i+1,j+1}\right)$
i,j+1/2	$\left(y_{i,j+1} - y_{i+1,j+1}\right)$	$\left(x_{i+1,j+1} - x_{i,j+1}\right)$
i-1/2,j	$\left(y_{i,j+1} - y_{i,j}\right)$	$-\left(x_{i,j+1} - x_{i,j}\right)$

Table 1: Normalized values of s_x and s_y.

The metric terms to this generalized coordinate system are defined as:

$$h_x = S_{x\_int}/V_{int}\ ,\ \ h_y = S_{y\_int}/V_{int} \quad \text{and} \quad h_n = S/V_{int}\ . \tag{6}$$

The properties calculated at the flux interface are obtained either by arithmetical average or by Roe (1981) average. In this work, the arithmetical average was used:

$$\rho_{\text{int}} = 0.5(\rho_R + \rho_L),\ u_{\text{int}} = 0.5(u_R + u_L),\ v_{\text{int}} = 0.5(v_R + v_L) \ \text{ and } \ H_{\text{int}} = 0.5(H_R + H_L). \tag{7}$$

$$a_{\text{int}} = \sqrt{(\gamma - 1)\left[H_{\text{int}} - 0.5\left(u_{\text{int}}^2 + v_{\text{int}}^2\right)\right]}, \tag{8}$$

where a_{int} is the speed of sound at the flux interface. The eigenvalues of the Euler equations, in the ξ direction, are given by:

$$U_{cont} = u_{int}h_x + v_{int}h_y,\ \ \lambda_1 = U_{cont} - a_{int}h_n,\ \ \lambda_2 = \lambda_3 = U_{cont} \quad \text{and} \quad \lambda_4 = U_{cont} + a_{int}h_n\ . \tag{9}$$

The jumps of the conserved variables, necessary to the construction of the Yee, Warming and Harten (1982) dissipation function, are given by:

$$\Delta e = V_{\text{int}}(e_R - e_L),\ \Delta\rho = V_{\text{int}}(\rho_R - \rho_L),\ \Delta(\rho u) = V_{\text{int}}[(\rho u)_R - (\rho u)_L] \ \text{ and } \ \Delta(\rho v) = V_{\text{int}}[(\rho v)_R - (\rho v)_L]. \tag{10}$$

The α vectors at the *(i+½,j)* interface are calculated by the following expressions:

$$\alpha^1 = 0.5(aa - bb),\ \alpha^2 = \Delta\rho - aa\ ,\ \alpha^3 = cc \quad \text{and} \quad \alpha^4 = 0.5(aa + bb). \tag{11}$$

with:

$$aa = \frac{(\gamma - 1)}{a_{\text{int}}^2}\left[\Delta e + 0.5\left(u_{\text{int}}^2 + v_{\text{int}}^2\right)\Delta\rho - u_{\text{int}}\Delta(\rho u) - v_{\text{int}}\Delta(\rho v)\right]; \tag{12}$$

$$bb = \frac{1}{a_{\text{int}}}\left[h_x'\Delta(\rho u) - \left(h_x'u_{\text{int}} + h_y'v_{\text{int}}\right)\Delta\rho + h_y'\Delta(\rho v)\right]; \tag{13}$$

$$cc = h_x'\Delta(\rho v) + \left(h_y'u_{\text{int}} - h_x'v_{\text{int}}\right)\Delta\rho - h_y'\Delta(\rho u); \tag{14}$$

$$h_x' = h_x/h_n \quad \text{and} \quad h_y' = h_y/h_n\ . \tag{15}$$

The Yee, Warming and Harten (1982) dissipation function uses the right-eigenvector matrix of the normal to the flux face Jacobian matrix in generalized coordinates:

$$R_{i+1/2,j} = \begin{bmatrix} 1 & 1 & 0 & 1 \\ u_{\text{int}} - h_x'a_{\text{int}} & u_{\text{int}} & -h_y' & u_{\text{int}} + h_x'a_{\text{int}} \\ v_{\text{int}} - h_y'a_{\text{int}} & v_{\text{int}} & h_x' & v_{\text{int}} + h_y'a_{\text{int}} \\ H_{\text{int}} - h_x'u_{\text{int}}a_{\text{int}} - h_y'v_{\text{int}}a_{\text{int}} & 0.5\left(u_{\text{int}}^2 + v_{\text{int}}^2\right) & h_x'v_{\text{int}} - h_y'u_{\text{int}} & H_{\text{int}} + h_x'u_{\text{int}}a_{\text{int}} + h_y'v_{\text{int}}a_{\text{int}} \end{bmatrix}. \tag{16}$$

Two options to the ψ_l entropy function, responsible to guarantee that only relevant physical solutions are to be considered, are implemented aiming an entropy satisfying algorithm:

$$\nu_l = \Delta t\lambda_l = Z_l \quad \text{and} \quad \psi_l = Z_l^2 + 0.25\,; \tag{17}$$

Or:

$$\psi_l = \begin{cases} |Z_l|, & \text{if } |Z_l| \geq \delta_f \\ 0.5\left(Z_l^2 + \delta_f^2\right)/\delta_f\,, & \text{if } |Z_l| < \delta_f \end{cases}, \tag{18}$$

where "*l*" varies from 1 to 4 (two-dimensional space) and δ_f assuming values between 0.1 and

0.5, being 0.2 the value recommended by Yee, Warming and Harten (1982). In the present studies, Eq. (17) was used to perform the numerical experiments.

The $\widetilde{g}$ function at the *(i+½,j)* interface is defined by:

$$\widetilde{g}^{l} = 0.5\left(\psi_{l} - Z_{l}^{2}\right)\alpha^{l}. \tag{19}$$

The *g* numerical flux function, which is a limited function to avoid the formation of new extremes in the solution and is responsible to the second order accuracy of the scheme, is given by:

$$g_{i,j}^{l} = signal_{l} \times MAX\left(0.0; MIN\left(\left|\widetilde{g}_{i+1/2,j}^{l}\right|, \widetilde{g}_{i-1/2,j}^{l} \times signal_{l}\right)\right), \tag{20}$$

where $signal_l$ is equal to 1.0 if $\widetilde{g}_{i+1/2,j}^{l} \geq 0.0$ and -1.0 otherwise.

The θ term, responsible to the artificial compression, which enhances the resolution of the scheme at discontinuities, is defined as follows:

$$\theta_{i,j}^{l} = \begin{cases} \left|\alpha_{i+1/2,j}^{l} - \alpha_{i-1/2,j}^{l}\right| \Big/ \left(\left|\alpha_{i+1/2,j}^{l}\right| + \left|\alpha_{i-1/2,j}^{l}\right|\right), & if \ \left|\alpha_{i+1/2,j}^{l}\right| + \left|\alpha_{i-1/2,j}^{l}\right| \neq 0.0 \\ 0.0, & if \ \left|\alpha_{i+1/2,j}^{l}\right| + \left|\alpha_{i-1/2,j}^{l}\right| = 0.0 \end{cases}; \tag{21}$$

The β parameter at the *(i+½,j)* interface, which introduces the artificial compression term in the algorithm, is given by the following expression:

$$\beta_{l} = 1.0 + \omega_{l} MAX(\theta_{i,j}^{l}, \theta_{i+1,j}^{l}), \tag{22}$$

in which ω_l assumes the following values: $\omega_1 = 0.25$ (non-linear field), $\omega_2 = \omega_3 = 1.0$ (linear field) and $\omega_4 = 0.25$ (non-linear field). The numerical characteristic speed, φ_l, at the *(i+½,j)* interface, which is responsible to transport the numerical information associated to the g numerical flux function, is defined by:

$$\varphi_{l} = \begin{cases} \left(g_{i+1,j}^{l} - g_{i,j}^{l}\right) \Big/ \alpha^{l}, & if \ \alpha^{l} \neq 0.0 \\ 0.0, & if \ \alpha^{l} = 0.0 \end{cases}. \tag{23}$$

The entropy function is redefined considering φ_l and β_l: $Z_l = \nu_l + \beta_l \varphi_l$, and ψ_l is recalculated according to Eq. (17) or to Eq. (18). Finally, the Yee, Warming and Harten (1982) dissipation function, to second order of spatial accuracy, is constructed by the following matrix-vector product:

$$\left\{D_{YWH}\right\}_{i+1/2,j} = \left[R\right]_{i+1/2,j} \left\{\left(\beta\left(g_{i,j} + g_{i+1,j}\right) - \psi\alpha\right) \Big/ \Delta t_{i,j}\right\}_{i+1/2,j}. \tag{24}$$

The convective numerical flux vector to the *(i+½,j)* interface is described by:

$$F_{i+1/2,j}^{(l)} = \left(E_{int}^{(l)} h_x + F_{int}^{(l)} h_y\right) V_{int} + 0.5 D_{YWH}^{(l)}, \tag{25}$$

with:

$$E_{int}^{(l)} = 0.5\left(E_{R}^{(l)} + E_{L}^{(l)}\right) \quad \text{and} \quad F_{int}^{(l)} = 0.5\left(F_{R}^{(l)} + F_{L}^{(l)}\right). \tag{26}$$

The time integration follows the time splitting method, first order accurate, which divides the integration in two steps, each one associated with a specific spatial direction. In the initial step, it is possible to write:

$$\Delta Q^{*}_{i,j} = -\Delta t / V_{i,j} \left(F^{n}_{i+1/2,j} - F^{n}_{i-1/2,j} \right); \quad Q^{*}_{i,j} = Q^{n}_{i,j} + \Delta Q^{*}_{i,j}; \tag{27}$$

and in the final step:

$$\Delta Q^{n+1}_{i,j} = -\Delta t / V_{i,j} \left(F^{*}_{i,j+1/2} - F^{*}_{i,j-1/2} \right); \quad Q^{n+1}_{i,j} = Q^{*}_{i,j} + \Delta Q^{n+1}_{i,j}. \tag{28}$$

A first order method was implemented as time integrator because only steady state solutions are aimed and, with it, time accurate solutions are not intended.

4 HARTEN (1983) ALGORITHM

The Harten (1983) algorithm, second order accurate in space, follows the Eqs. (4) to (16). The next step is the definition of the entropy condition, which is defined by Eq. (17), ν_l, and Eq. (18).

The $\tilde{g}$ function at the *(i+½,j)* interface is defined according to Eq. (19) and the g numerical flux function is given by Eq. (20). The numerical characteristic speed φ_l at the *(i+½,j)* interface is defined according to Eq. (23).

The entropy function is redefined considering φ_l: $Z_l = \nu_l + \varphi_l$, and ψ_l is recalculated according to Eq. (18). Finally, the Harten (1983) dissipation function, to second order spatial accuracy, is constructed by the following matrix-vector product:

$$\left\{ D_{Harten} \right\}_{i+1/2,j} = \left[R \right]_{i+1/2,j} \left\{ \left(g_{i,j} + g_{i+1,j} - \psi\alpha \right) / \Delta t_{i,j} \right\}_{i+1/2,j}. \tag{29}$$

Equations (25) and (26) are used to conclude the numerical flux vector of the Harten (1983) scheme and the time integration is performed by the time splitting method defined by Eqs. (27) and (28).

5 YEE AND KUTLER (1985) ALGORITHM

The Yee and Kutler (1985) algorithm, second order accurate in space, follows Eqs. (4) to (16). The next step consists in determining the θ function. This function is defined in terms of the differences of the gradients of the characteristic variables to take into account discontinuities effects and is responsible to artificial compression:

$$\theta^{l}_{i,j} = \begin{cases} \dfrac{\left| \alpha^{l}_{i+1/2,j} - \alpha^{l}_{i-1/2,j} \right|}{\alpha^{l}_{i+1/2,j} + \alpha^{l}_{i-1/2,j}}, & if \left(\alpha^{l}_{i+1/2,j} + \alpha^{l}_{i-1/2,j} \right) \neq 0.0 \\ 0.0, & if \left(\alpha^{l}_{i+1/2,j} + \alpha^{l}_{i-1/2,j} \right) = 0.0 \end{cases}. \tag{30}$$

The κ function at the *(i+½,j)* interface is defined as follows:

$$\kappa_l = 1/8 \left(1 + \omega_l MAX\left(\theta^{l}_{i,j}, \theta^{l}_{i+1,j} \right) \right), \tag{31}$$

The *g* numerical flux function is determined by:

$$g^{l}_{i,j} = signal_l \times MAX\left(0,0; MIN\left(\left| \alpha^{l}_{i+1/2,j} \right|, \alpha^{l}_{i-1/2,j} \times signal_l \right) \right), \tag{32}$$

where $signal_l$ assumes value 1.0 if $\alpha^{l}_{i+1/2,j} \geq 0.0$ and -1.0 otherwise. The numerical characteristic speed φ_l at the *(i+½,j)* interface is calculated by the following expression:

$$\varphi_l = \begin{cases} \kappa_l \left(g^l_{i+1,j} - g^l_{i,j} \right) / \alpha^l , & if\ \alpha^l \neq 0.0 \\ 0.0, & if\ \alpha^l = 0.0 \end{cases} . \tag{33}$$

The ψ_l entropy function at the *(i+½,j)* interface is defined by:

$$\psi_l = \left(\nu_l + \varphi_l \right)^2 + 0.25 , \tag{34}$$

with ν_l defined according to Eq. (17). Finally, the Yee and Kutler (1985) dissipation function, to second order spatial accuracy, is constructed by the following matrix-vector product:

$$\left\{ D_{Yee/Kutler} \right\}_{i+1/2,j} = \left[R \right]_{i+1/2,j} \left\{ \left(\kappa \left(g_{i,j} + g_{i+1,j} \right) - \psi \alpha \right) / \Delta t_{i,j} \right\}_{i+1/2,j} . \tag{35}$$

Equations (25) and (26) are used to conclude the numerical flux vector of Yee and Kutler (1985) scheme and the time integration is performed by the time splitting method defined by Eqs. (27) and (28).

6 HUGHSON AND BERAN (1991) ALGORITHM

The Hughson and Beran (1991) algorithm, second order accurate in space, follows Eqs. (4) to (16). The next step consists in determining the g numerical flux function. To non-linear fields (l = 1 and 4), it is possible to write:

$$g^l_{i,j} = \begin{cases} \dfrac{\alpha^l_{i+1/2,j} \alpha^l_{i-1/2,j} + \left| \alpha^l_{i+1/2,j} \alpha^l_{i-1/2,j} \right|}{\alpha^l_{i+1/2,j} + \alpha^l_{i-1/2,j}}, & if\ \left(\alpha^l_{i+1/2,j} + \alpha^l_{i-1/2,j} \right) \neq 0.0 . \\ 0.0, & if\ \left(\alpha^l_{i+1/2,j} + \alpha^l_{i-1/2,j} \right) = 0.0 \end{cases} \tag{36}$$

To linear fields (l = 2 and 3), it is possible to write:

$$g^l_{i,j} = signal_l \times MAX\left(0.0; MIN\left(\left| \alpha^l_{i-1/2,j} \right|, \alpha^l_{i+1/2,j} \times signal_l \right) \right), \tag{37}$$

where $signal_l$ is equals to 1.0 if $\alpha^l_{i-1/2,j} \geq 0.0$ and -1.0 otherwise. After that, Equations (17) , ν_l term, and (18) are employed and the σ_l term at the *(i+½,j)* interface is defined:

$$\sigma_l = 0.5 \left(\psi_l - Z_l^2 \right). \tag{38}$$

The φ_l numerical characteristic speed at the *(i+½,j)* interface is defined by:

$$\varphi_l = \begin{cases} \sigma_l \left(g^l_{i+1,j} - g^l_{i,j} \right) / \alpha^l , & if\ \alpha^l \neq 0.0 \\ 0.0, & if\ \alpha^l = 0.0 \end{cases} . \tag{39}$$

The entropy function is redefined considering the φ_l term: $Z_l = \nu_l + \varphi_l$ and ψ_l is recalculated according to Eq. (18). Finally, the Hughson and Beran (1991) dissipation function, to second order accuracy in space, is constructed by the following matrix-vector product:

$$\left\{ D_{Hughson/Beran} \right\}_{i+1/2,j} = \left[R \right]_{i+1/2,j} \left\{ \left(\sigma \left(g_{i,j} + g_{i+1,j} \right) - \psi \alpha \right) / \Delta t_{i,j} \right\}_{i+1/2,j} . \tag{40}$$

Equations (25) and (26) are used to conclude the numerical flux vector of Hughson and Beran (1991) scheme and the time integration is performed by the time splitting method defined by Eqs. (27) and (28).

7 SPATIALLY VARIABLE TIME STEP

The basic idea of this procedure consists in keeping constant the CFL number in all calculation domain, allowing, hence, the use of appropriated time steps to each specific mesh region during the convergence process. Hence, according to the definition of the CFL number, it is possible to write:

$$\Delta t_{i,j} = CFL(\Delta s)_{i,j} / c_{i,j} , \tag{41}$$

where CFL is the "Courant-Friedrichs-Lewy" number to provide numerical stability to the scheme; $c_{i,j} = \left[\left(u^2 + v^2\right)^{0.5} + a\right]_{i,j}$ is the maximum characteristic speed of information propagation in the calculation domain; and $(\Delta s)_{i,j}$ is a characteristic length of information transport. On a finite volume context, $(\Delta s)_{i,j}$ is chosen as the minor value found between the minor centroid distance, involving the *(i,j)* cell and a neighbor, and the minor cell side length.

8 INITIAL AND BOUNDARY CONDITIONS

8.1 Initial condition

To the physical problems studied in this work, freestream flow values are adopted for all properties as initial condition, in the whole calculation domain (Jameson and Mavriplis, 1986, and Maciel, 2002). Therefore, the vector of conserved variables is defined as:

$$Q_{i,j} = \left\{ 1 \quad M_\infty \cos\alpha \quad M_\infty \sin\alpha \quad \frac{1}{\gamma(\gamma - 1)} + 0.5 M_\infty^2 \right\}^T , \tag{42}$$

being M_∞ the freestream flow Mach number and α the flow attack angle.

8.2 Boundary conditions

The boundary conditions are basically of three types: solid wall, entrance and exit. These conditions are implemented in special cells named ghost cells.

(a) Wall condition: This condition imposes the flow tangency at the solid wall. This condition is satisfied considering the wall tangent velocity component of the ghost volume as equals to the respective velocity component of its real neighbor cell. At the same way, the wall normal velocity component of the ghost cell is equaled in value, but with opposite signal, to the respective velocity component of the real neighbor cell.

The pressure gradient normal to the wall is assumed be equal to zero, following an inviscid formulation. The same hypothesis is applied to the temperature gradient normal to the wall, considering adiabatic wall. The ghost volume density and pressure are extrapolated from the respective values of the real neighbor volume (zero order extrapolation), with these two conditions. The total energy is obtained by the state equation of a perfect gas.

(b) Entrance condition:

(b.1) Subsonic flow: Three properties are specified and one is extrapolated, based on analysis of information propagation along characteristic directions in the calculation domain (Maciel and Azevedo, 1998, and Maciel, 2002). In other words, three characteristic directions of information propagation point inward the computational domain and should be specified. Only the characteristic direction associated to the "*(q_n-a)*" velocity can not be specified and should be determined by interior information of the calculation domain. The pressure was the

extrapolated variable from the real neighbor volume, to the studied problems. Density and velocity components had their values determined by the freestream flow properties. The total energy per unity fluid volume is determined by the state equation of a perfect gas.
(b.2) Supersonic flow: All variables are fixed with their freestream flow values.
(c) Exit condition:
(c.1) Subsonic flow: Three characteristic directions of information propagation point outward the computational domain and should be extrapolated from interior information (Maciel and Azevedo, 1998, and Maciel, 2002). The characteristic direction associated to the "$(q_n\text{-}a)$" velocity should be specified because it penetrates the calculation domain. In this case, the ghost volume's pressure is specified by its freestream value. Density and velocity components are extrapolated and the total energy is obtained by the state equation of a perfect gas.
(c.2) Supersonic flow: All variables are extrapolated from the interior domain due to the fact that all four characteristic directions of information propagation of the Euler equations point outward the calculation domain and, with it, nothing can be fixed.

9 RESULTS

Tests were performed in a CELERON-1.2GHz and 128 Mbytes of RAM memory microcomputer. Converged results occurred to 4 orders of reduction in the value of the maximum residual. The maximum residual is defined as the maximum value obtained from the discretized conservation equations. The value used to γ was 1.4. To all problems, the attack angle was adopted equal to 0.0°.

In the present results, the following nomenclature is used to represent the studied schemes:
YWH – Represent Yee, Warming and Harten (1982) solutions;
H - Represent Harten (1983) solutions;
YK - Represent Yee and Kutler (1985) solutions;
HB - Represent Hughson and Beran (1991) solutions.

9.1 Ramp physical problem

To this physical problem, an algebraic mesh with 61x100 points was used, which is composed of 5,940 rectangular volumes and of 6,100 nodes, on a finite volume context. The ramp configuration is described in Fig. 2. It was adopted a freestream Mach number of 2.0 as initial condition, characterizing a supersonic flow regime.

Figures 3 to 6 exhibit the density field obtained by the Yee, Warming and Harten (1982), the Harten (1983), the Yee and Kutler (1985) and the Hughson and Beran (1991) schemes, respectively. It is possible to note that the density field generated by the Hughson and Beran (1991) scheme is the densest in relation to the others schemes. The density fields generated by the Yee, Warming and Harten (1982) scheme and by the Yee and Kutler (1985) scheme are the same, as many in quantitative terms as in qualitative terms.

Figures 7 to 10 show the pressure field obtained by the Yee, Warming and Harten (1982), the Harten (1983), the Yee and Kutler (1985) and the Hughson and Beran (1991) schemes, respectively. The pressure field generated by the Hughson and Beran (1991) scheme is the most severe in relation to the others schemes. It is interesting to note that the Hughson and Beran (1991) and the Harten (1983) solutions present a red region (bigger pressure values) with the same size, when compared the pressure contours. These regions are bigger than the equivalent regions obtained by the Yee, Warming and Harten (1982) and the Yee and Kutler (1985) schemes.

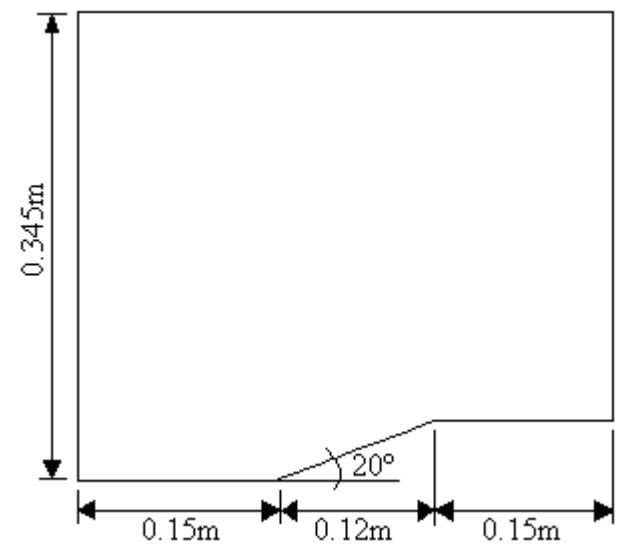

Figure 2: Ramp configuration.

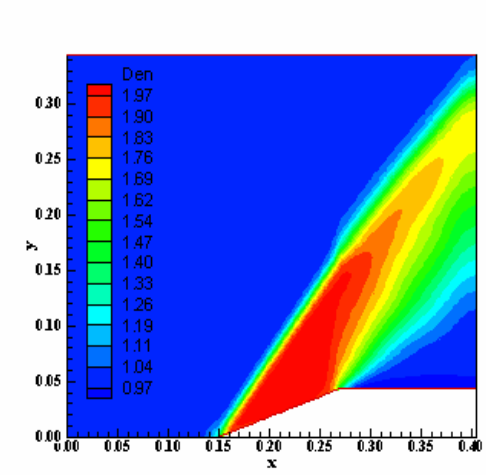

Figure 3: Density field (YWH).

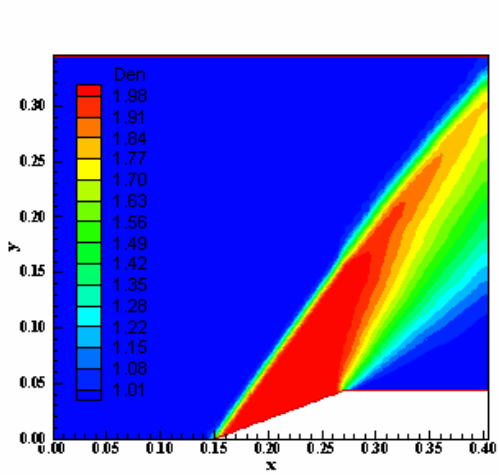

Figure 4: Density field (H).

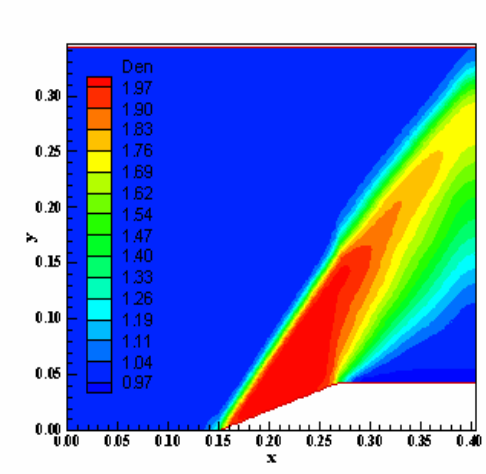

Figure 5: Density field (YK).

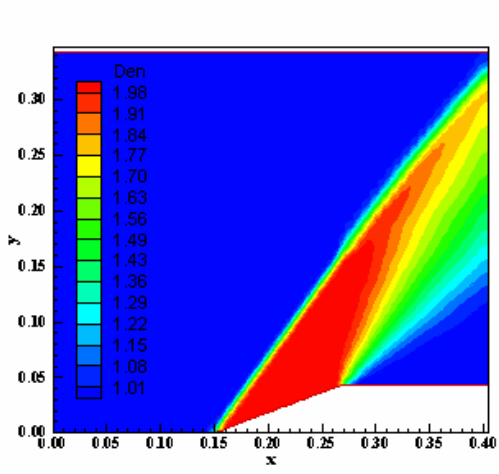

Figure 6: Density field (HB).

Moreover, the Yee, Warming and Harten (1982) and the Yee and Kutler (1985) schemes

present again the same solution. Although differences exist between the algorithms, both schemes have the same behavior in this example. Equations (21) and (22) behave in the same way as Eqs. (30) and (31), respectively. The different ways of providing artificial compression, which enhances the discontinuity resolution, have the same effects in this problem to these schemes.

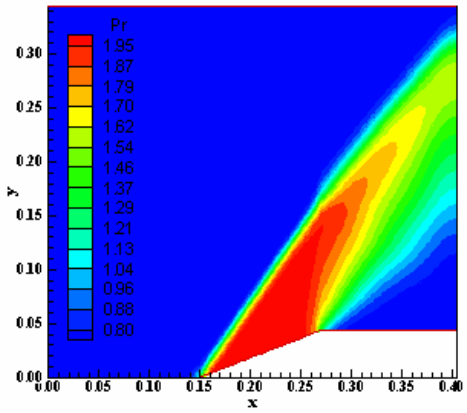

Figure 7: Pressure field (YWH).

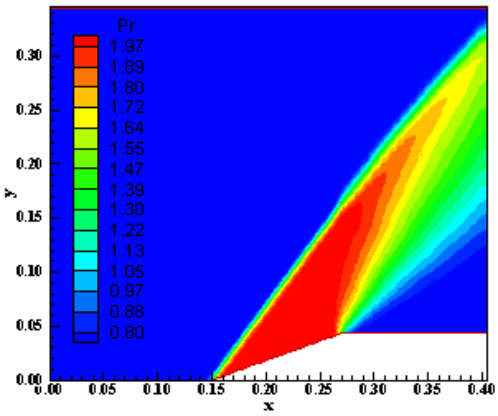

Figure 8: Pressure field (H).

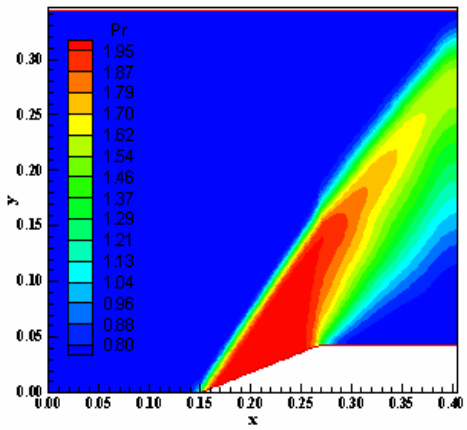

Figure 9: Pressure field (YK).

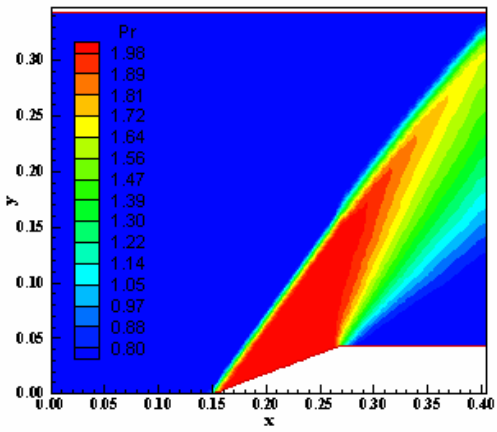

Figure 10: Pressure field (HB).

Figures 11 to 14 exhibit the Mach number field generated by the Yee, Warming and Harten (1982), the Harten (1983), the Yee and Kutler (1985) and the Hughson and Beran (1991) schemes, respectively. The Mach number contours generated by the Hughson and Beran (1991) scheme is the most intense field in relation to the others schemes. The Hughson and Beran (1991) and the Harten (1983) schemes present again areas of more intense Mach numbers (blue area) extended in longer regions than the Yee, Warming and Harten (1982) and the Yee and Kutler (1985) schemes.

Figure 15 shows the pressure distributions along the ramp obtained by the Yee, Warming and Harten (1982), the Harten (1983), the Yee and Kutler (1985) and the Hughson and Beran (1991) schemes. They are compared with the exact solutions from oblique shock theory and the Prandtl-Meyer expansion wave theory.

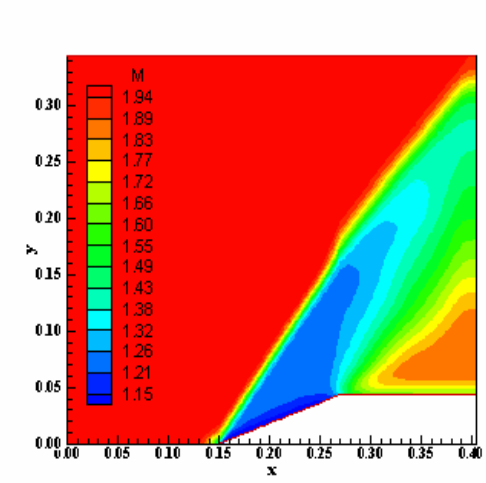

Figure 11: Mach number field (YWH).

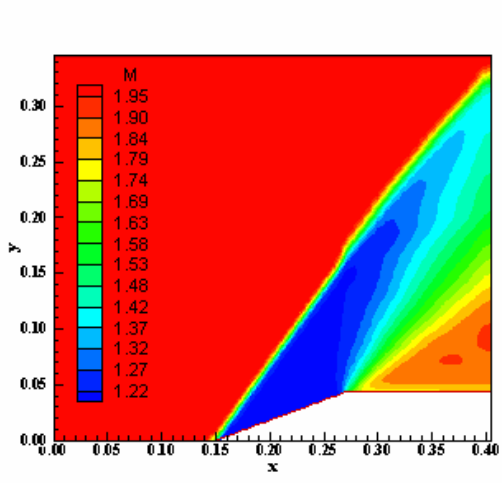

Figure 12: Mach number field (H).

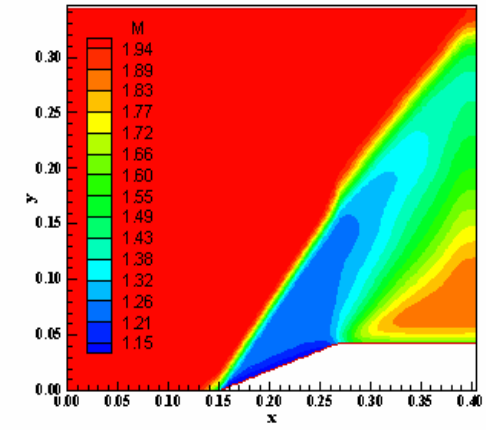

Figure 13: Mach number field (YK).

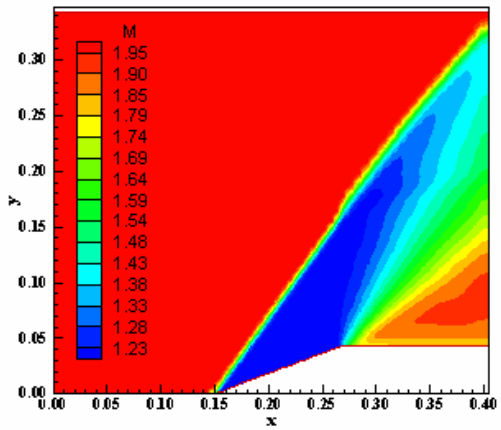

Figure 14: Mach number field (HB).

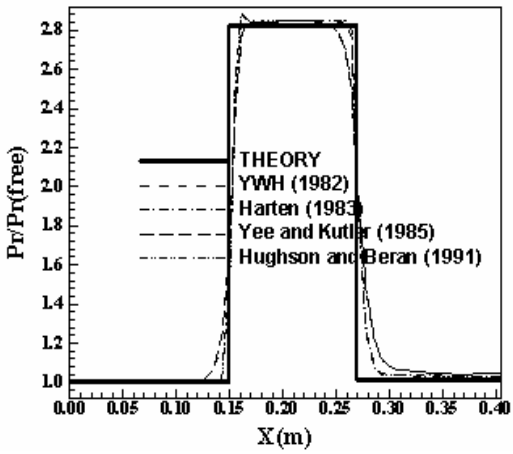

Figure 15: Wall pressure distributions.

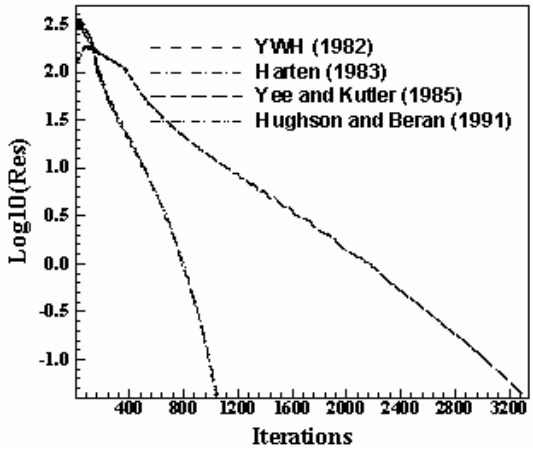

Figure 16: Convergence histories.

It is possible to note that the solutions generated by the Yee, Warming and Harten (1982) and the Yee and Kutler (1985) schemes are smoother than those generated by the Harten (1983) and the Hughson and Beran (1991) schemes, but they do not present oscillations at the shock

region, what characterizes better solutions, in qualitative terms, than the Harten (1983) and the Hughson and Beran (1991) ones. They are doing what is expected to high resolution schemes do: solutions of second order schemes free of oscillations at shock regions. In the solutions generated by the Harten (1983) and the Hughson and Beran (1991) schemes, the shock presents a small peak in relation to the theory, but the shock is sharp defined and the expansion fan is less smoothed. The Hughson and Beran (1991) scheme presents the most critical value of pressure at the ramp beginning, the shock position. All schemes overpredict the value of the pressure at the ramp (at the plateau region) in relation to the theoretical solution. The width of the constant pressure region after the shock (the plateau) at the ramp is better represented by the Harten (1983) and by the Hughson and Beran (1991) schemes, as also the pressure at the end of the expansion fan, after the ramp. The Yee, Warming and Harten (1982) and the Yee and Kutler (1985) schemes also presents the same solution in terms of pressure distribution.

Figure 16 exhibits the convergence history obtained by the Yee, Warming and Harten (1982), the Harten (1983), the Yee and Kutler (1985) and the Hughson and Beran (1991) schemes. The Harten (1983) and the Hughson and Beran (1991) schemes requires only one-third of the iterations that the Yee, Warming and Harten (1982) and the Yee and Kutler (1985) schemes need to convergence. All histories are approximately linear and without meaningful oscillations.

Other way to quantitatively verify if the solutions generated by each scheme are satisfactory consists in determining the shock angle of the oblique shock wave, β, measured in relation to the initial direction of the flow field. Anderson (1984) (pages 352 and 353) presents a diagram with values of the shock angle, β, to oblique shock waves. The value of this angle is determined as function of the freestream Mach number and of the deflection angle of the flow after the shock wave, ϕ. To $\phi = 20^{o}$ (ramp inclination angle) and to a freestream Mach number equals to 2.0, it is possible to obtain from this diagram a value to β equals to 53.0^{o}. Using a transfer in Figures 7, 8, 9 and 10, it is possible to obtain the values of β to each scheme, as well the respective errors, shown in Tab. 1. Hence, the results highlight that the Harten (1983) scheme is the most accurate of the studied schemes.

Algorithm:	β:	Error (%):
Yee, Warming and Harten (1982)	55.0	3.8
Harten (1983)	54.0	1.9
Yee and Kutler (1985)	54.5	2.8
Hughson and Beran (1991)	54.5	2.8

Table 1: Shock angle and percentage errors.

9.2 Blunt body physical problem

To this physical problem, an algebraic mesh with 103x100 points or composed of 10,098 rectangular volumes and 10,300 nodes was used. The far field was located at 20 times the curvature ratio of the blunt body nose. An exponential stretching of 5% was implemented in the η direction. The blunt body configuration is described in Fig. 17.

The freestream Mach number adopted for this simulation as initial condition was 5.0, characterizing a supersonic flow regime.

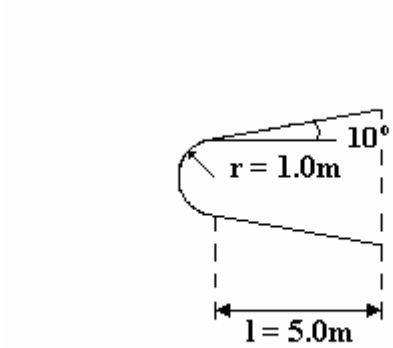

Figure 17: Blunt body configuration.

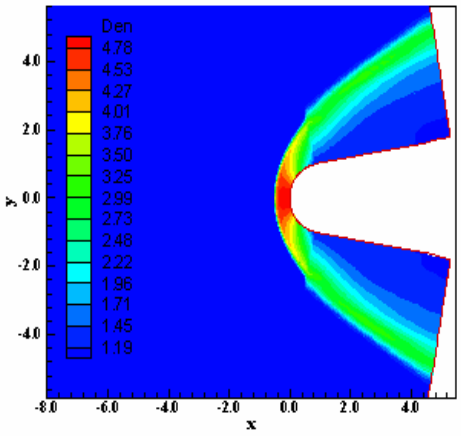

Figure 18: Density field (YWH).

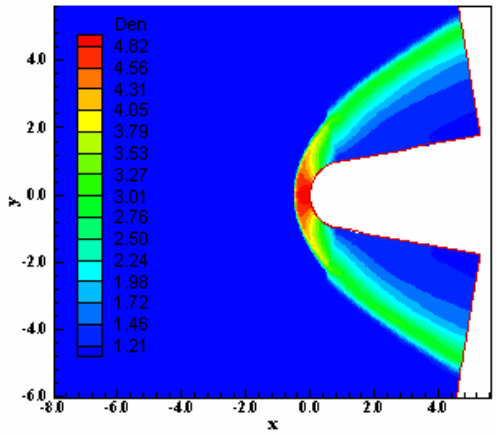

Figure 19: Density field (H).

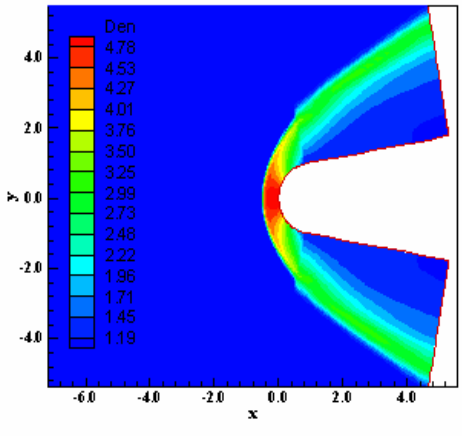

Figure 20: Density field (YK).

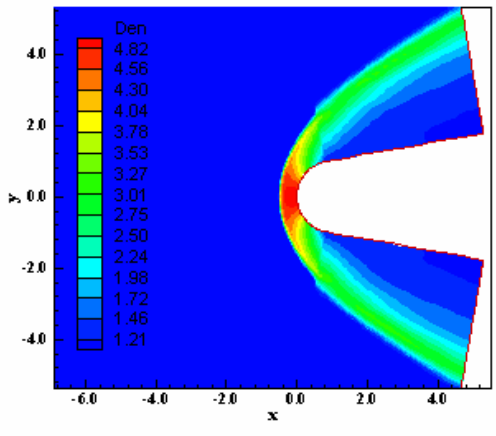

Figure 21: Density field (HB).

Figures 18 to 21 exhibit the density field generated by the Yee, Warming and Harten (1982), the Harten (1983), the Yee and Kutler (1985) and the Hughson and Beran (1991) algorithms, respectively. The density distribution generated by the Harten (1983) scheme is the densest in relation to the others schemes. The Yee, Warming and Harten (1982) and the Yee and Kutler (1985) solutions are the same. All solutions present good symmetry properties

in relation to the blunt body.

Figures 22 to 25 show the pressure field generated by the Yee, Warming and Harten (1982), by the Harten (1983), by the Yee and Kutler (1985) and by the Hughson and Beran (1991) schemes, respectively. The pressure field generated by the Harten (1983) scheme is the most severe in relation to the others schemes. Good symmetry properties are again observed in all solutions.

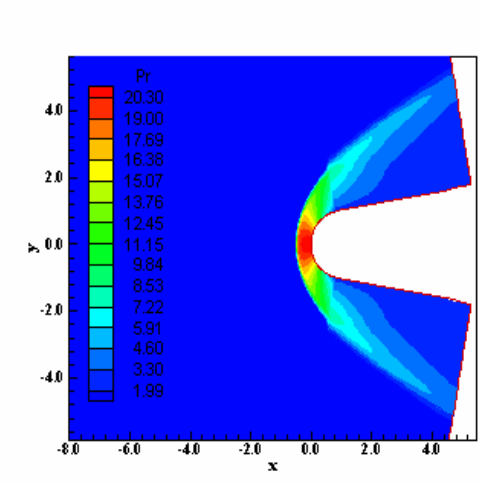

Figure 22: Pressure field (YWH).

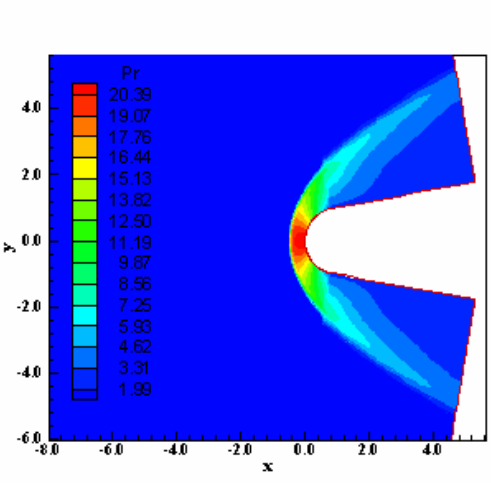

Figure 23: Pressure field (H).

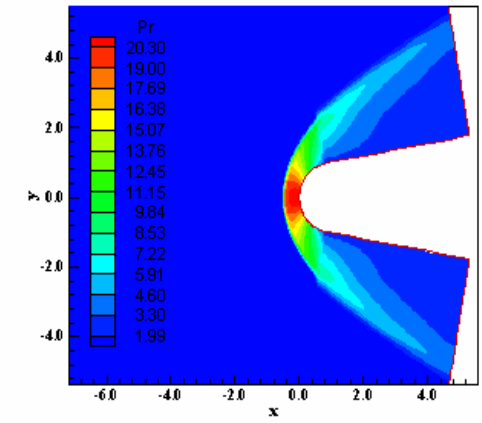

Figure 24: Pressure field (YK).

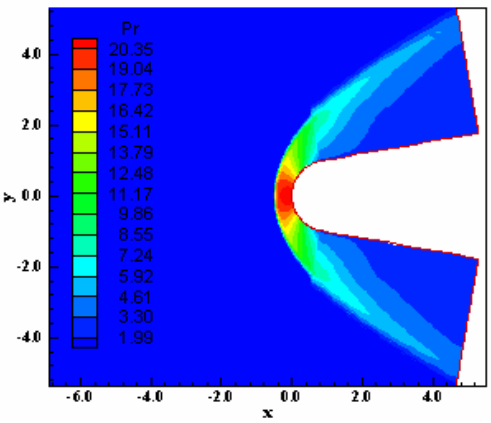

Figure 25: Pressure field (HB).

Figures 26 to 29 exhibit the Mach number field obtained by the Yee, Warming and Harten (1982), the Harten (1983), the Yee and Kutler (1985) and the Hughson and Beran (1991) schemes, respectively. The Mach number fields are practically the same in quantitative terms, presenting some differences in qualitative aspects.

Table 2 exhibits the aerodynamic coefficients of lift and drag obtained by each scheme. As can be seen, the most correct value of c_L was obtained by the solutions generated by the Harten (1983) and by the Hughson and Beran (1991) schemes. It tends to zero due to the symmetry of the geometry and due to the zero value of the attack angle.

Figure 30 shows the -Cp distributions around the blunt body geometry obtained by the schemes. There are no meaningful differences among the solutions generated by the algorithms, with all solutions obtaining the same value to the Cp peak at the configuration

nose (Cp = 1.68). Figure 31 exhibits the convergence histories of the studied schemes.

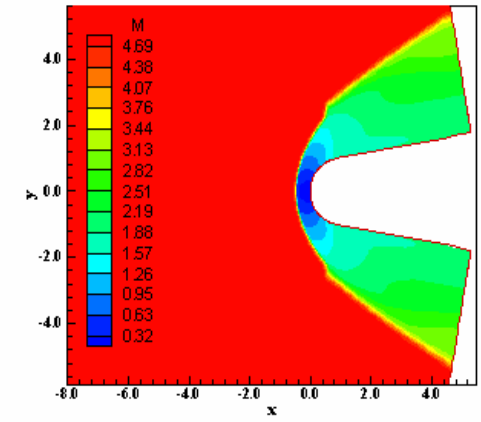

Figure 26: Mach number field (YWH).

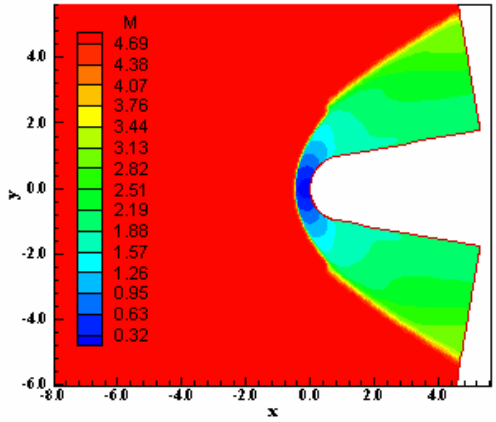

Figure 27: Mach number field (H).

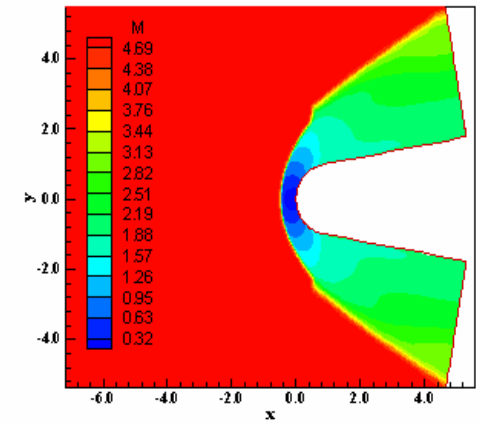

Figure 28: Mach number field (YK).

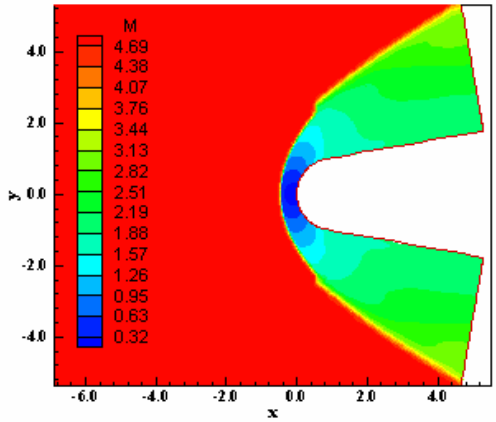

Figure 29: Mach number field (HB).

Algorithm:	c_L:	c_D:
Yee, Warming and Harten (1982)	4.0×10^{-4}	9.7×10^{-5}
Harten (1983)	-1.3×10^{-4}	4.3×10^{-5}
Yee and Kutler (1985)	4.0×10^{-4}	8.7×10^{-5}
Hughson and Beran (1991)	1.3×10^{-4}	5.3×10^{-5}

Table 2: Values of the aerodynamic coefficients c_L and c_D.

Another possibility to quantitative comparison of all schemes is the determination of the stagnation pressure ahead of the configuration. Anderson (1984) presents a table of normal shock wave properties in its B Appendix. This table permits the determination of some shock wave properties as function of the freestream Mach number. In front of the blunt body configuration, the shock wave presents a normal shock behavior, which permits the determination of the stagnation pressure, behind the shock wave, from the tables encountered in Anderson (1984). It is possible to determine the ratio pr_0 / pr_∞ from Anderson (1984), where pr_0 is the stagnation pressure in front of the configuration and pr_∞ is the freestream

pressure (equals to 1/γ with this nondimensionalization).

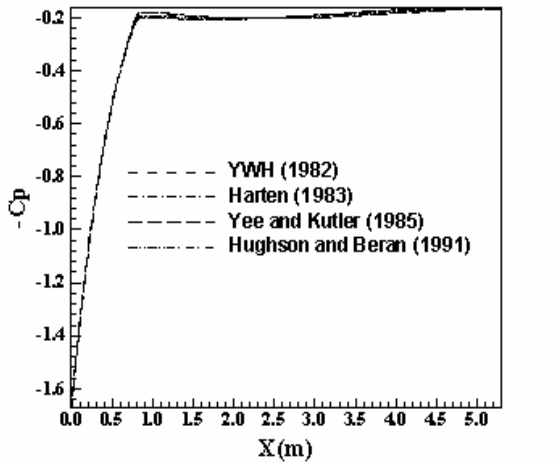

Figure 30: -Cp distributions.

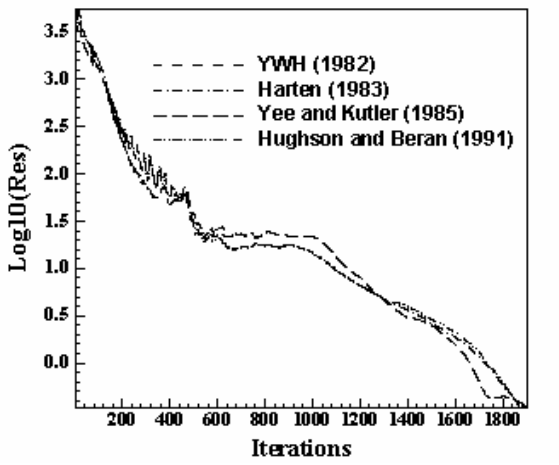

Figure 31: Convergence histories.

Hence, to this problem, $M_\infty = 5.0$ corresponds to $pr_0 / pr_\infty = 32.65$ and remembering that $pr_\infty = 0.714$, it is possible to conclude that $pr_0 = 23.31$. Values of the stagnation pressure, with respective percentage errors, to each scheme are shown in Tab. 3. As can be seen, the Harten (1983) scheme yielded again the best result in terms of accuracy.

Algorithm:	pr_0:	Error (%):
Yee, Warming and Harten (1982)	20.30	12.9
Harten (1983)	20.39	12.5
Yee and Kutler (1985)	20.30	12.9
Hughson and Beran (1991)	20.35	12.7

Table 3: Values of the stagnation pressure and percentage errors.

With the results of the ramp and of the blunt body, two schemes are better than the others. The solutions generated by the Hughson and Beran (1991) scheme in the ramp problem are the most critical in relation to the others schemes, while the Harten (1983) scheme yields the most accurate results in both problems and the most critical results in the blunt body problem.

9.3 Numerical data of the simulations

	Ramp problem		Blunt body problem		
Algorithm:	CFL:	Iterations:	CFL:	Iterations:	Cost*:
Yee, Warming and Harten (1982)	0.3	3,348	0.9	1,906	0.0000755
Harten (1983)	0.9	1,059	0.9	1,885	0.0000494
Yee and Kutler (1985)	0.3	3,348	0.9	1,906	0.0000083
Hughson and Beran (1991)	0.9	1,042	0.9	1,876	0.0000541

* Measured in seconds/per volume/per iteration.

Table 4. Numerical data of the simulations.

Table 4 presents the data of the numerical experiments involving the supersonic flow along the ramp and around the blunt body studied in this work. It is possible to note that the Yee and Kutler (1985) scheme is the cheapest scheme, approximately 810% less expensive than the Yee, Warming and Harten (1982) scheme, the most expensive.

10 CONCLUSIONS

The present work compares the flux difference splitting TVD algorithms of Yee, Warming and Harten (1982), of Harten (1983), of Yee and Kutler (1985) and of Hughson and Beran (1991), all schemes second order accurate in space, applied to aeronautical and aerospace problems in the two-dimensional space. The Euler equations, on a finite volume context, using an upwind and a structured spatial discretization, were solved. A spatially variable time step was employed to accelerate the convergence process to the steady state solution. The gains in terms of convergence ratio with this procedure were highlighted in Maciel (2005). The steady state physical problems of the supersonic flows along a ramp and around a blunt body configuration were solved.

All schemes have presented good solutions in qualitative and quantitative terms. In the ramp problem, the Hughson and Beran (1991) scheme was the most critical because presented the most severe pressure field and the most intense Mach number field in relation to the others schemes. The shock and the expansion fan are better captured by the Yee, Warming and Harten (1982) and the Yee and Kutler (1985) schemes, although smoother than the solutions generated by the Harten (1983) and the Hughson and Beran (1991) schemes, which presented a shock peak. The Harten (1983) and the Hughson and Beran (1991) schemes presented better pressure distribution than the others schemes when compared with the theory. The shock angle was best estimated by the Harten (1983) scheme. In the blunt body problem, the Harten (1983) scheme presented the most severe pressure field in relation to the others schemes, characterizing the most critical solution. The Mach number and the -Cp distributions of all schemes were practically the same. The aerodynamic coefficient of lift was better estimated in the solutions generated by the Harten (1983) and the Hughson and Beran (1991) schemes. The stagnation pressure in front of the configuration nose is best determined by the Harten (1983) scheme. The Yee and Kutler (1985) scheme, the cheapest scheme, is about 810% less expensive than the Yee, Warming and Harten (1982) scheme, the most expensive. The Yee, Warming and Harten (1982) and the Yee and Kutler (1985) schemes have presented the same solutions, where the different forms of defining the artificial compression terms of both schemes do not present meaningful differences. A more complete study, with more physical problems, will be accomplished by this author aiming to better highlight the characteristics of these schemes.

As conclusion, the Harten (1983) scheme presents the most accurate solutions in comparison with the others schemes in both examples studied in this work, as well the most severe pressure field in the blunt body problem, high supersonic flow, characterizing it as the most conservative in relation to the others schemes to this type of flow, which indicates this one as a good scheme to the prediction of flow properties in the project phase of aerospace vehicles.

Most critical or most severe solutions were characterized as the solutions which presented the biggest values of pressure in the pressure field generated by the schemes or the biggest value of Cp, which represents again biggest values of pressure. The pressure is the reference variable because it determines the level of the main dynamic effort which the configuration is submitted.

REFERENCES

J. D. Anderson. *Fundamentals of Aerodynamics*. McGraw-Hill, Inc., EUA, 563p, 1984.

A. Harten. High Resolution Schemes for Hyperbolic Conservation Laws. *Journal of Computational Physics*, 49: 357-393, 1983.

M. C. Hughson and P. S. Beran. Analysis of Hyperbolic Blunt-Body Flows Using a Total Variation Diminishing (TVD) Scheme and the MacCormack Scheme. *AIAA 91-3206-CP*, 1991.

A. Jameson and D. Mavriplis. Finite Volume Solution of the Two-Dimensional Euler Equations on a Regular Triangular Mesh. *AIAA Journal*, 24: 611-618, 1986.

R. W. MacCormack. The Effect of Viscosity in Hypervelocity Impact Cratering. *AIAA Paper 69-354*, 1969.

E. S. G. Maciel. Simulação Numérica de Escoamentos Supersônicos e Hipersônicos Utilizando Técnicas de Dinâmica dos Fluidos Computacional. *Doctoral Thesis*, ITA, CTA, São José dos Campos, SP, Brazil, 258p, 2002.

E. S. G. Maciel. Analysis of Convergence Acceleration Techniques Used in Unstructured Algorithms in the Solution of Aeronautical Problems – Part I. *Proceedings of the XVIII International Congress of Mechanical Engineering (XVIII COBEM)*, Ouro Preto, MG, Brazil, 2005.

E. S. G. Maciel and J. L. F. Azevedo. Comparação entre Vários Algoritmos Implícitos de Fatoração Aproximada na Solução das Equações de Navier-Stokes. *RBCM – Journal of the Brazilian Society of Mechanical Sciences*, Brazil, XX (3): 353-380, 1998.

P. L. Roe. Approximate Riemann Solvers, Parameter Vectors, and Difference Schemes. *Journal of Computational Physics*. 43: 357-372, 1981.

H. C. Yee and P. Kutler. Application of Second-Order-Accurate Total Variation Diminishing (TVD) Schemes to the Euler Equations in General Geometries. *NASA-TM-85845*, 1985.

H. C. Yee, R. F. Warming and A. Harten. A High-Resolution Numerical Technique for Inviscid Gas-Dynamic Problems with Weak Solutions. *Proceedings of the 8th International Conference on Numerical Methods in Fluid Dynamics*, E. Krause, Editor, Lecture Notes in Physics, Springer-Verlag, Berlim, Germany, 170: 546-552, 1982.